Predicted properties of OB star - black hole binaries

Bachelorarbeit in Physik

von
Katja Stoll

angefertigt im Argelander-Institut für Astronomie

vorgelegt der
Mathematisch-Naturwissenschaftlichen Fakultät

der Universität Bonn

Februar 2019

Ich versichere, dass ich diese Arbeit selbständig verfasst und keine anderen als die angegebenen Quellen und Hilfsmittel benutzt sowie die Zitate kenntlich gemacht habe.

Bonn, den ..... Unterschrift .....

1. Gutachter: Prof. Dr. Norbert Langer
2. Gutachter: Prof. Dr. Frank Bertoldi

Contents

1 Introduction

The detection of gravitational waves from the merger of two massive black holes (BH) by the Laser Interferometer Gravitational-Wave Observatory (Abbott et al. (2016)) opened up new possibilities of understanding the theory of gravity and the evolution of massive stars. It is therefore of high interest to examine the progenitor systems of these BH + BH mergers. As only massive progenitor stars can lead to such high mass BHs, these stars are likely to spend their main sequence lifetime as a star of spectral type O or B. This means that the systems resulting in a BH + BH merger must have spent a certain time as an OB star + BH system.
Because it is a great challenge to detect these systems, we use a binary star data grid in this thesis to investigate the properties of the OB star + BH systems and derive the probability for OB stars to have a BH companion dependent on observable parameters like mass and radial velocity.

2 Theory

2.1 The evolution of massive stars[1]

Observational data suggests that stars are formed out of molecular clouds which fragment into smaller pieces, the protostellar cores. These continue to collapse and accrete gas which leads to an increase in temperature. When the accretion stops and the temperature in the core is high enough for nuclear fusion, the star stops contracting and settles on the zero-age main sequence (ZAMS).

An object may be called a star if it is bound by its own gravity and radiates energy from an internal source. This results in a lower limit for the mass of a star which is set by the stellar core not being hot enough to ignite hydrogen in a stable burning process. At the other extreme, the mass of a star is limited by the Eddington luminosity, at which radiation pressure begins to push away the outer layers of the star.
The initial mass distribution function of main-sequence stars can be approximated by the power-law (Salpeter (1955))

$$\frac{\mathrm{d}N}{\mathrm{d}M} \propto M^{-2.35}. \tag{1}$$

Observations show that the mass of a main-sequence star is clearly correlated with its luminosity, higher mass stars having a much higher luminosity

$$L \propto M^3. \tag{2}$$

This means that the higher the mass of a star, the shorter is its main-sequence lifetime, as massive stars burn hydrogen to helium much faster in order to provide such higher luminosities.

[1] This section is based on the lecture notes by Pols (2009).

The further evolution of a star after hydrogen is exhausted in the core depends on its initial mass and it is useful to distinguish between low-mass stars (up to $\approx 8\,M_\odot$) and stars with masses exceeding $8\,M_\odot$, on which we want to focus in this thesis.
After hydrogen is exhausted in the core, the star starts to contract and the pressure and temperature in the central region increase. Hydrogen ignites in a shell around the core which contracts further on until the temperature is high enough for helium to ignite. The burning shell appears to act like a mirror, meaning that the contraction of the core results in an expansion of the envelope.
This process repeats for helium burning. Massive stars reach a sufficiently high temperature in their cores to burn carbon stably in a non-degenerate core. Once carbon is ignited, the further evolution is sped up enormously due to strong neutrino losses. The process of contraction, shell burning of the previous main burning element and ignition of a heavier element repeats several times until the formation of an iron core. As iron has the highest binding energy per nucleon, nuclear fusion cannot provide energy any more and the core collapses into a neutron star or a black hole.

2.2 Mass transfer in binary systems[2]

Important parameters for the evolution of binary stars are their orbital separation and the mass ratio. As stars expand during their evolution, it may happen that a star transfers mass to its binary companion, depending on the mentioned initial parameters of the system. This mass transfer leads to a change in other physical properties of the system besides the mass, such as the angular momentum and surface abundances. Very close systems may even result in a merger. There are systems however, that have such a wide orbit that no interaction takes place and both stars evolve as single stars.

Whether a system would interact and exchange mass or not is defined by the Roche potential. Most important is the region within which the matter is still bound to the respective component, called Roche lobe. When the radius of the initially more massive star (the primary star) which evolves faster than the secondary, less massive star, becomes equal to its Roche radius (the radius of a sphere with the volume of the Roche lobe), we define the start of a Roche-lobe overflow (RLOF). We can therefore distinguish between detached (non-interacting) systems, semi-detached systems for which one of the stars overflows its Roche lobe and contact systems with both components overflowing their Roche lobes.

For the parameters of the OB star + BH system, it plays a key role in which evolutionary stage the RLOF happened. Binaries that start to interact during their main sequence evolution are referred to as case A systems. If mass transfer sets in when the primary has already left the main sequence and evolved towards the red giant branch, we speak of a case B system. For those systems, the primary is typically stripped of its entire hydrogen envelope leaving only the exposed helium core.

[2]This section is based on the first three chapters of Postnov and Yungelson (2014).

3 Methods

3.1 Grids of binary evolution models

In this work we use the grids of binary evolution models by Marchant (2016). They contain detailed numerical simulations of binary stars in the Large Magellanic Cloud performed with the stellar evolution code MESA (Modules for Experiments in Stellar Astrophysics) by Paxton et al. (2011). The masses of the primary stars range from $\log(M_1/M_\odot) = 1.000$ ($M_1 = 10\,M_\odot$) to $\log(M_1/M_\odot) = 1.600$ ($M_1 \approx 39.81\,M_\odot$) in steps of $\log(M_1/M_\odot) = 0.050$. For each primary mass, systems with different mass ratios $q = \frac{M_2}{M_1}$ ranging from 0.025 to 0.975 in intervals of 0.025 are computed and for each mass ratio, there are models with orbital periods of $\log(P/d)$ from 0.150 ($P \approx 1.4\,d$) to 3.500 ($P \approx 3162\,d$) in steps of 0.025.

The models are computed assuming tidal synchronisation at the ZAMS, i. e. without an additional parameter for the initial rotation. The systems are evolved until central carbon depletion (or helium depletion for stars with helium core masses larger than $M = 14\,M_\odot$ due to convergence problems) unless one of the following criteria for different mass transfer scenarios cause the simulation to stop. In the cases of an overflow of the outer Lagrangian point L2, inverse mass transfer in a binary with a post main sequence component, a system reaching the upper $\dot{M}$ limit (the material unable to be accreted by the secondary cannot be expelled and a common envelope is formed), mass transfer in a system with $q_i < 0.25$ or the occurrence of a convergence error, it is assumed that the stars of the concerned system merge. When the primary reaches core carbon depletion, the simulation terminates assuming the primary leaves the secondary, which is evolved as a single star further on.

Common envelope ejection due to a transfer of energy and angular momentum from the two stars orbiting around their center of mass to the envelope is possible but not modelled. Therefore this effect cannot be considered here even though it may result in a close BH + BH binary.

3.2 Selection of the OB star + BH systems

Whether a system would evolve into an OB star + BH binary depends on the mass of the primary star in its late evolutionary stages. As the time for the evolution after core carbon depletion is negligibly short (see Section 2.1), we evaluate the properties of the binary system at the last time step computed by MESA which corresponds to carbon depletion for the systems taken into account.

According to Sukhbold et al. (2018), the helium and CO core masses of presupernova stars increase approximately linearly with the mass of the concerned star at the ZAMS (see right panel of Figure 1). Based on the criteria by Ertl et al. (2016) and Müller et al. (2016), the left panel of Figure 1 shows whether a model with a certain mass at the ZAMS is expected to explode as a supernova rather than collapse to a black hole.

To maximise the number of systems taken into account for our considerations that will actually evolve into a black hole through core collapse, we exclude all the stars with a mass of $M \lesssim 20.1\,M_\odot$ at the ZAMS. This corresponds to a helium core mass in the presupernova stage of evolution of $M_{He} \approx 6.6\,M_\odot$. Therefore we take all those systems into account for which the primary evolves into a star that depletes carbon in the core with a helium core mass of $M_{He} > 6.6\,M_\odot$ at a time when the secondary star is still in its main sequence evolution, meaning that its central hydrogen mass fraction is still more than 1 %. We assume that the star collapses directly into a BH without losing any mass due to a kick.

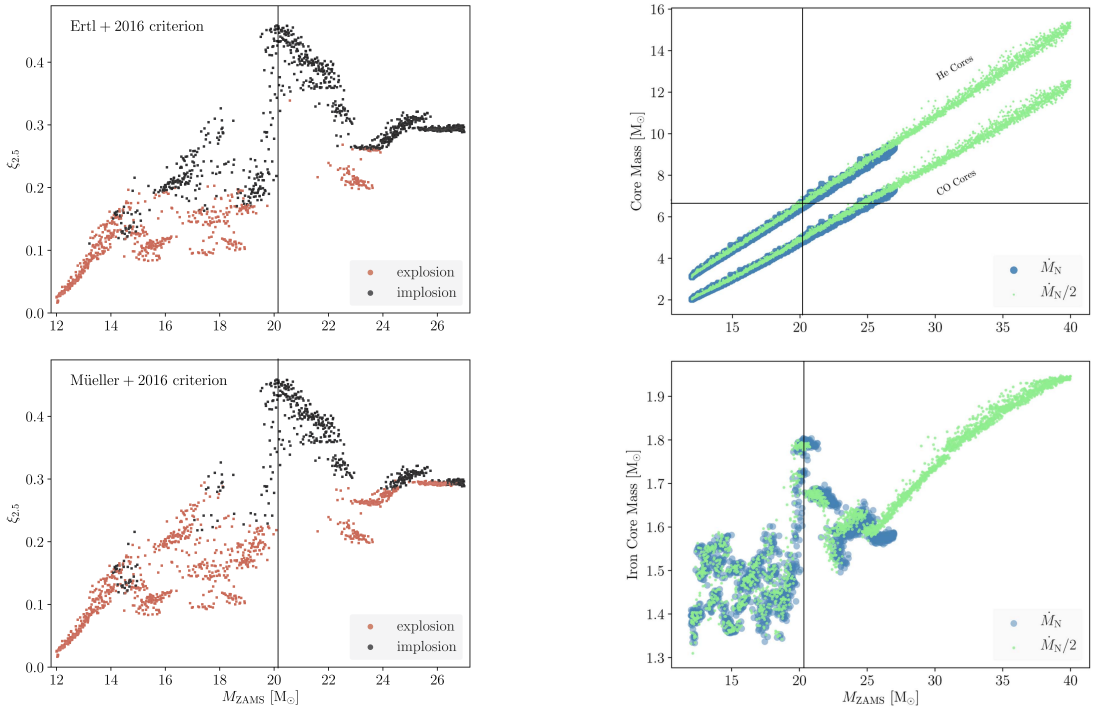

Figure 1: (left) Red symbols denote a successful supernova explosion, black symbols denote a collapse to a black hole according to the criteria of Ertl et al. (2016) (top) and Müller et al. (2016) (bottom). Systems to the left of the horizontal black line at $M \approx 20.1\,M_\odot$ are meant to be excluded for our considerations.
(right) Helium, CO (top) and Fe (bottom) core masses for presupernova stars as a function of the mass at ZAMS. The ZAMS mass of $M \approx 20.1\,M_\odot$ corresponds to a helium core mass of $M_{He} \approx 6.6\,M_\odot$.
Both figures are taken from Sukhbold et al. (2018).

3.3 Statistical weight

In order to take into account the actual frequency of stars with different initial parameters we need to consider initial distribution functions. As mentioned in Section 2.1, the initial mass distribution can be described by Equation 1. Furthermore, we use initial distributions for mass ratio and orbital period as Sana et al. (2012),

$$\frac{\mathrm{d}N}{\mathrm{d}q} \propto q^{-0.1}, \tag{3}$$

$$\frac{\mathrm{d}N}{\mathrm{d}\log\left(\frac{P}{d}\right)} \propto \left(\log\left(\frac{P}{d}\right)\right)^{-0.55}. \tag{4}$$

We consider these functions drawing random number triples distributed according to the initial distribution functions and assigning them to the system in the grid whose initial parameters are closest to the drawn triple. We can thus weigh each system by the resulting probability to derive the likelihood to observe a certain binary system. Through this weighting, systems with a lower initial mass, mass ratio and orbital period have a higher probability.

3.4 Computation of the radial velocity

We aim to give the observer an idea of the parameters of the visible star for which it is most likely to have a BH as a companion. As the radial velocity is an important observational parameter which is not included in the direct output of the MESA data, we derived a relation between the semi-amplitude of the radial velocity, the orbital period P of the system and the masses of the two components using Kepler's third law

$$P^2 = \frac{4\pi^2}{GM}a^3, \tag{5}$$

where G is the gravitational constant, $M = m_1 + m_2$ the total mass of the system and $a = a_1 + a_2$ the semi-major axis. Assuming a circular orbit and that the line of sight is edge-on with the orbital plane, the radial velocity semi-amplitude K_2 of the secondary star equals its orbital velocity $v_2 = \frac{2\pi}{P} \cdot a_2$. Furthermore, the equation $m_1 \cdot a_1 = m_2 \cdot a_2 = \frac{m_1 m_2}{m_1+m_2} \cdot a$ and thus $a = \frac{m_1+m_2}{m_1} \cdot a_2$ holds for the two-body system.

Using these relations, Equation 5 yields

$$K_2 = \left(\frac{2\pi G}{P}\right)^{\frac{1}{3}} \cdot \frac{m_1}{(m_1+m_2)^{\frac{2}{3}}}. \tag{6}$$

We can therefore compute the radial velocity semi-amplitude for each system at a certain point in time in its evolution.

4 Results

4.1 Evolutionary results of the binary systems

Figure 2 shows the results of the evolution for binary systems containing a primary star with an initial mass of $M = 31.62\,M_\odot$ depending on the initial mass ratio and orbital period of the system. Figures 23 to 29 in the appendix show the grids for those other primary star masses which contain systems that are further taken into account. As explained in Section 3.1, we expect all those systems to merge for which one of the following occurs: a convergence error happens, the upper $\dot{M}$ limit is reached, the mass ratio is below 0.25, the outer Lagrangian point L2 is overflowed during a contact phase or inverse mass transfer happens in a system with a post main-sequence component. These systems are not considered for our further calculations. Systems labelled with "BH+MS binary" fulfil the criteria to evolve into an OB star + BH system described in Section 3.2 and are taken into account for the further calculations. Systems labelled with "Both dep. C" are evolved up to carbon depletion but the primaries do either not reach a sufficiently high helium core mass or carbon is depleted at a point in time when the secondary has already left the main sequence.

Systems with a cross-hatched mark underwent a contact phase. For some cases this results in a merger but it is possible that models evolve into a semi-detached system after the period of contact. In this case, both components can evolve up to carbon depletion and the system results in an OB star + BH system which is considered for the further calculations. The striped mark denotes systems for which the limit on the mass loss rate comparing the total energy provided by radiation to the energy of the material lost by the donor star is reached. The models are evolved despite this happening, but radiation could be insufficient to expel the material unable to be accreted by the secondary star. Especially for the systems that either reach the upper $\dot{M}$ limit or terminate due to a convergence error, a common envelope ejection resulting in a close BH+BH system is possible, but not modelled.

4.2 Parameters of the OB star + BH systems

The resulting distribution function for the masses of the primaries at core carbon depletion is depicted in Figure 3. The integral over the total curve is normalised to one so that the fraction of systems in each bin compared to the total number of OB star + BH binaries can be read from the ordinate. Assuming that the helium core will collapse to a BH of the same mass, the resulting BH masses show a rather flat distribution ranging from $M_{BH} = 7\,M_\odot$ to $M_{BH} = 22\,M_\odot$.
To investigate the influence of mass transfer on the parameters of the OB star + BH binaries, we distinguished between systems undergoing case A mass transfer, those undergoing case B mass transfer and non-interacting systems. As certain features were identified as originating from the systems that underwent a contact phase, those are shown additionally as a histogram and are included in the distribution of case A mass transfer systems.

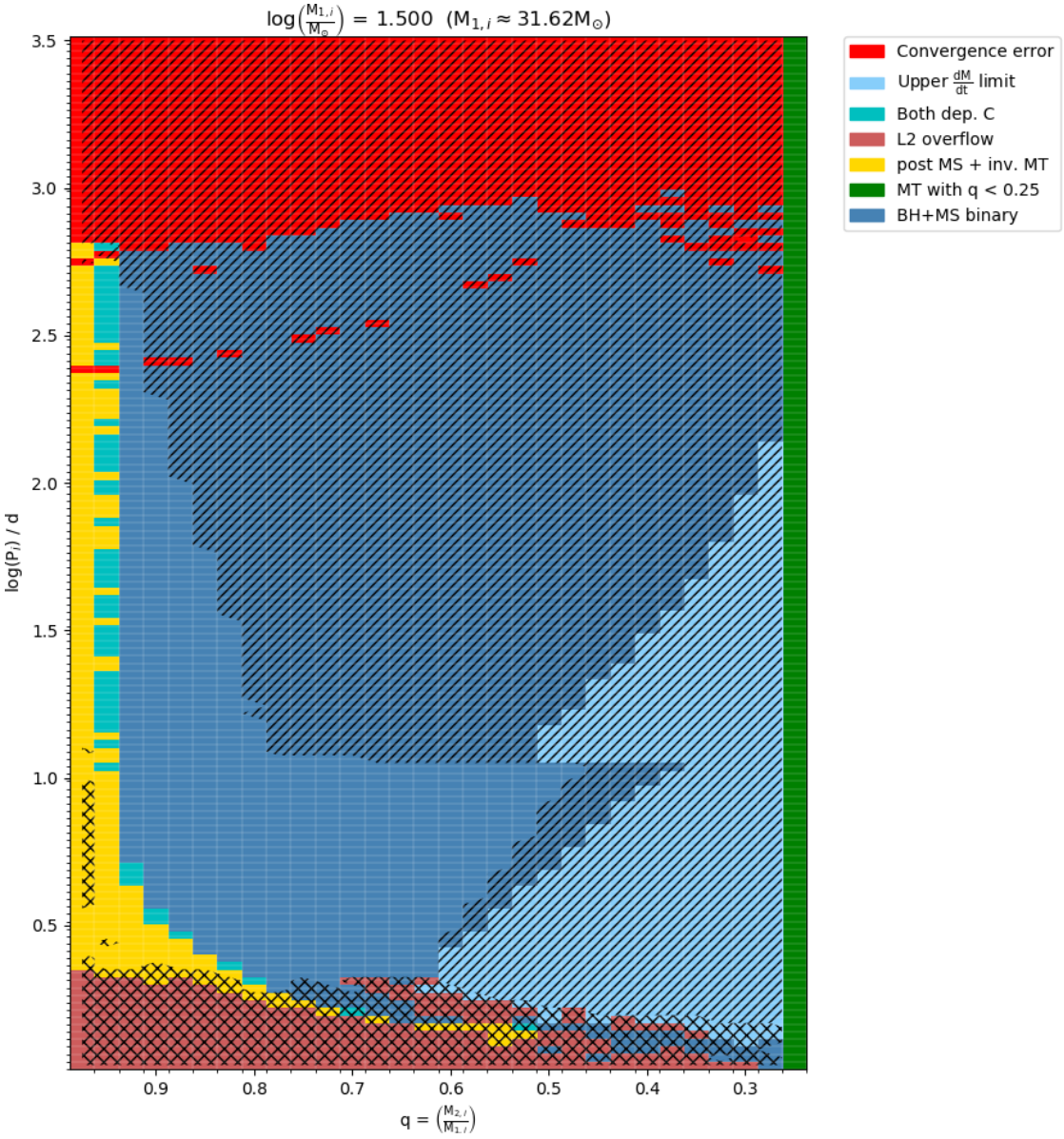

Figure 2: Grid of binary models for $\log\left(M_{1,i}/M_{\odot}\right) = 1.500$. All models indicated with dark blue are considered for our further calculations. See Section 4.1 for detailed explanation.

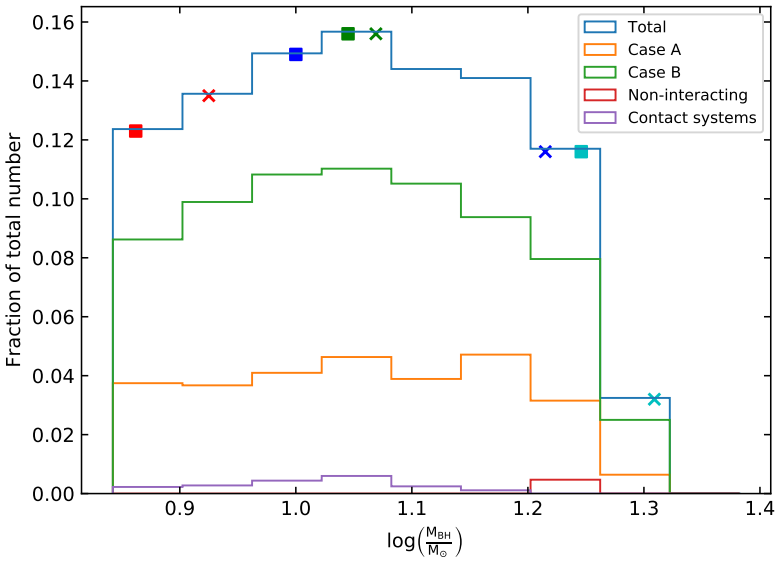

Figure 3: Distribution of the resulting BH masses. Initial distribution functions are taken into account according to Section 3.3. For parameters of the example systems see Table 1.

To see how individual systems are affected by binary evolution and which are the parameters of the resulting OB star + BH system in comparison to the total resulting distribution function, we depicted example systems (see Table 1 in the appendix for detailed properties of those) in each plot. Squares mark systems that underwent case A mass transfer, systems marked with a cross underwent case B mass transfer. The colours refer to the following initial parameters:

- Red: high q_i, low $\log(P_i/d)$
- Green: high q_i, high $\log(P_i/d)$
- Blue: low q_i, low $\log(P_i/d)$
- Cyan: low q_i, high $\log(P_i/d)$

Systems 1 and 2 (red) have a rather low initial primary mass, therefore the resulting BH mass is in the lower mass range too. Systems 7 and 8 (cyan) in contrast are taken from the grid with the highest initial primary mass and thus evolve into binaries with high black hole masses. In both cases, the model that underwent case B mass transfer has a higher BH mass than the case A system as the mass transfer efficiency is higher for case A mass transfer and the primary loses more mass to the accretor.

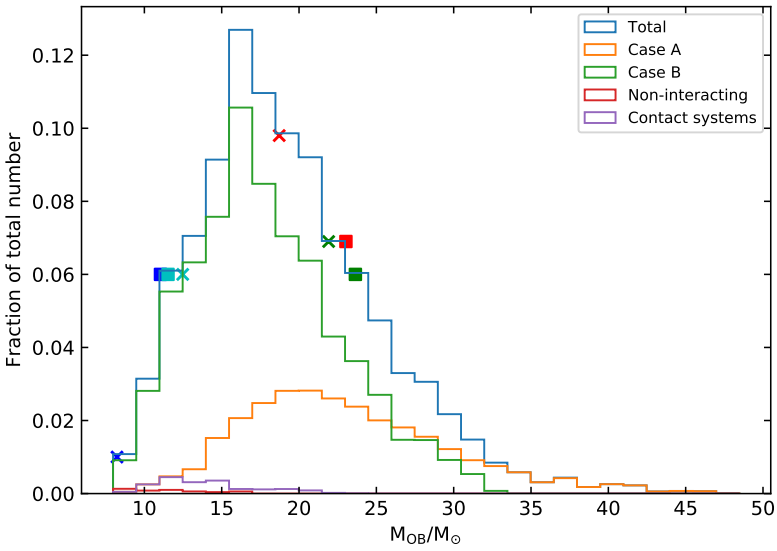

Figure 4: Distribution of the resulting OB star masses. Initial distribution functions are taken into account according to Section 3.3. For parameters of the example systems see Table 1.

Figure 4 shows the resulting distribution of OB star masses. It is a rather continuous distribution due to the different mass transfer efficiency for each system. As case B systems have accretion efficiencies less than 10 %, the OB stars masses are restricted to a certain value. Case A systems in contrast can have higher accretion efficiencies as tidal forces can prevent close systems from spin-up and reaching a critical rotational velocity. This results in a tail in the distribution for masses of $M_{OB} \gtrsim 32\,M_\odot$ due to OB stars that have accreted a high amount of mass. Because the number of models that evolve into an OB star + BH system increases with an increasing mass ratio there are less models with a low initial secondary mass. This is consistent with the increase in the number of systems with OB star masses from $M_{OB} \approx 9\,M_\odot$ to $M_{OB} \approx 16\,M_\odot$ in Figure 4.

In order to understand why the abundance of OB star masses decreases from $M_{OB} \approx 16\,M_\odot$ to $M_{OB} \approx 45\,M_\odot$ it is useful to examine the distribution of OB star masses that originate from a grid with a certain primary star mass as shown in Figure 5. In the grid with $M_{1,i} = 19.95\,M_\odot$, the majority of the models resulting in an OB star + BH system undergo case B mass transfer, most of the systems having a high initial mass ratio. We can observe that the resulting OB star mass is almost unaffected by a change in mass ratio and orbital period for $q_i > 0.800$ and $\log(P_i/d) > 1.000$. This suggests that the secondary stars in this grid can accrete mass up to a certain value of approximately $M \approx 18\,M_\odot$ but only few closer systems reach a higher mass. From the grids with initial primary masses of $M_{1,i} = 35.48\,M_\odot$ and $M_{1,i} = 39.81\,M_\odot$ in contrast, the OB

star masses are spread over almost the whole resulting mass range as systems with lower mass ratios also evolve into OB star + BH systems.

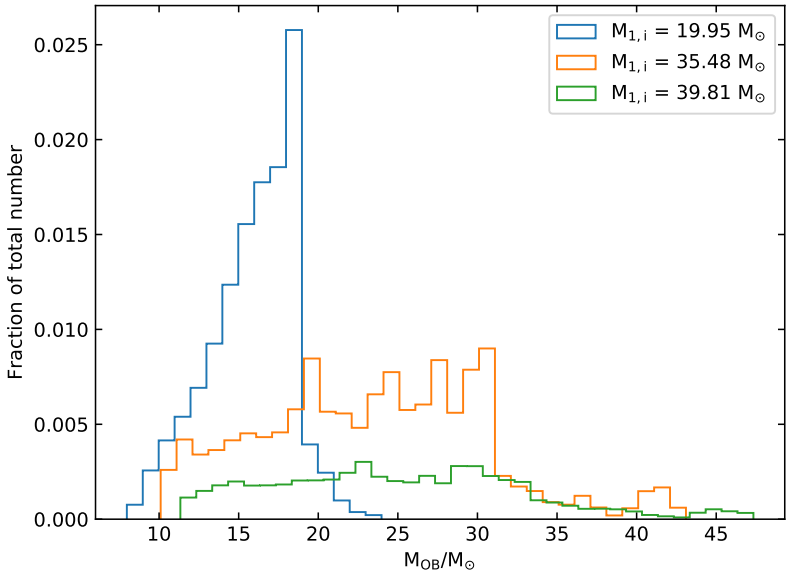

Figure 5: Distribution of the OB star masses. Depicted are only OB stars that originate from the grid with the indicated primary mass. Initial distribution functions are considered according to Section 3.3.

Therefore, there are fewer systems in one particular bin although the boundary at which only close binaries undergoing case A mass transfer reach a higher mass is still visible in the distribution for the grid with $M_{1,i} = 35.48\,M_\odot$. The weighting of the data favouring lower initial masses supports the decrease at higher OB star masses.

Figure 6 shows the resulting ratios of the OB star mass to the BH mass again under the assumption that the BH mass is equal to that of the helium core at carbon depletion. Mass ratios below one mean therefore that the systems consist of a relatively massive BH with an OB star as companion which is less massive. Systems with a mass ratio exceeding one consist of a lower mass BH with a more massive OB star. The tail at high mass ratios originates from case A systems with secondary stars accreting a high amount of mass and becoming much more massive than the primary star.

The orbital period distribution of the OB star + BH systems is shown in Figure 7. Four peaks are clearly distinguishable: the peak at low orbital periods coming from the contact systems that have evolved into very close systems, a peak originating from systems undergoing case A mass transfer at orbital periods with $0.5 \lesssim \log(P/d) \lesssim 1.2$, a third peak from case B systems with a relatively wide parameter range of $1.2 \lesssim \log(P/d) \lesssim 3.2$ and a fourth peak from the rather small number of non-interacting systems.

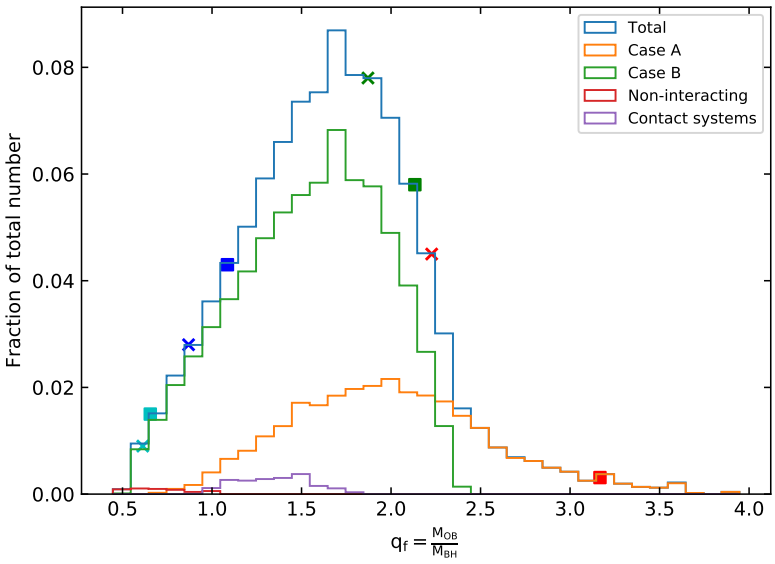

Figure 6: Distribution of the resulting mass ratios. Initial distribution functions are taken into account according to Section 3.3. For parameters of the example systems see Table 1.

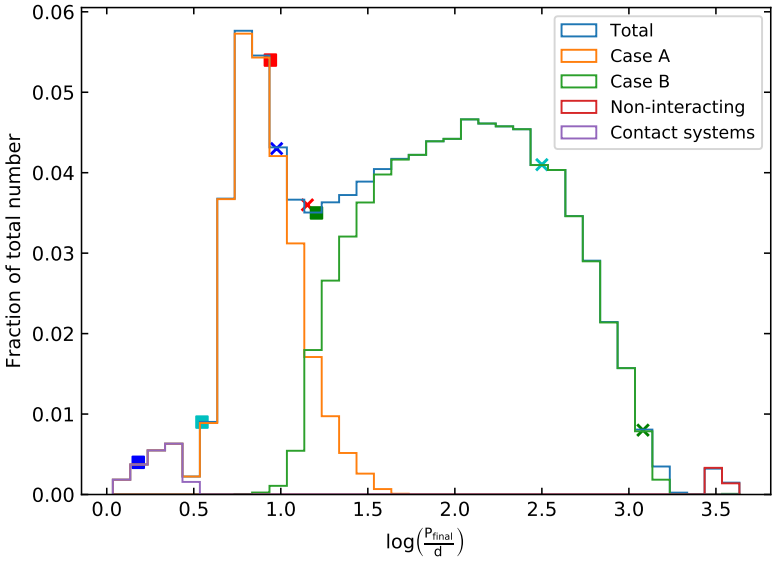

Figure 7: Distribution of the resulting orbital periods. Initial distribution functions are taken into account according to Section 3.3. For parameters of the example systems see Table 1.

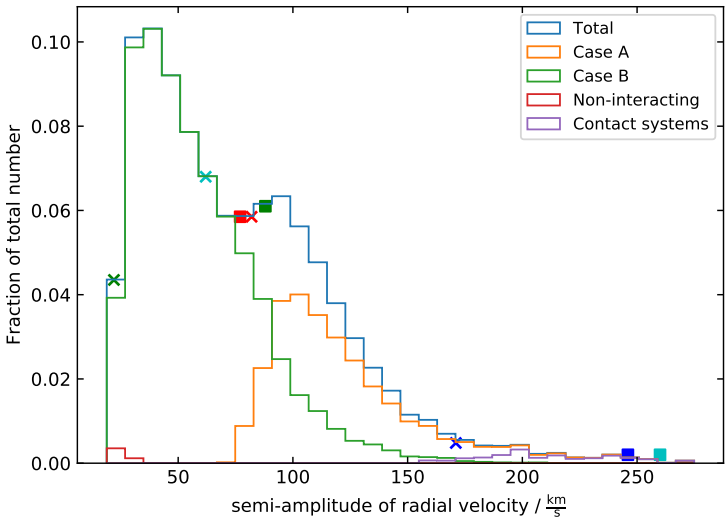

Figure 8: Distribution of the resulting radial velocity (computed according to Section 3.4). Initial distribution functions are taken into account according to Section 3.3. For parameters of the example systems see Table 1.

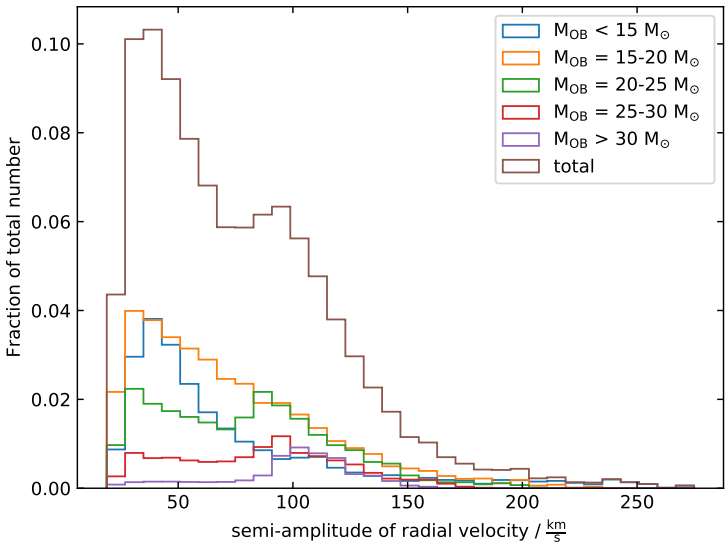

Figure 9: Distribution of the resulting radial velocity (computed according to Section 3.4) dependent on the mass of the OB star. Initial distribution functions are taken into account according to Section 3.3.

Figure 8 shows the distribution of the radial velocity semi-amplitude of the OB stars, which is computed according to Section 3.4. The distribution is consistent with that for the orbital period. For case B and non-interacting systems having a high orbital period, the radial velocity semi-amplitude of the OB star is rather low whereas case A and especially the contact systems being very close systems have a high radial velocity semi-amplitude.

In order to work out the mass dependency of the radial velocity, we split the systems into five groups of mass ranges of the OB stars as shown in Figure 9. We can state that the distributions for lower OB star masses ($M_{OB} < 15\,M_\odot$ and $M_{OB} = 15 - 20\,M_\odot$) show only a peak at lower radial velocity semi-amplitudes corresponding to the peak originating from case B systems. The distributions for OB star masses exceeding $20\,M_\odot$ in contrast show a second peak at higher radial velocities corresponding to the case A peak. This effect can be explained by the increasing number of systems undergoing case A mass transfer for an increasing initial mass of the primary which also means a higher initial mass possible for the secondary. This shows that we would expect a higher radial velocity semi-amplitude for a higher mass of the OB star.

4.3 Observation probabilities

In order to derive how likely it is that an observed OB star of a certain mass or radial velocity semi-amplitude is part of a binary with a BH, we have to take into account that the system would not spend its total lifetime as an OB star + BH binary but exists as a binary consisting of two main sequence stars before. Therefore, we compute the time until the primary reaches core carbon depletion as a fraction of the total lifetime (i. e. the time until the secondary reaches core carbon depletion) as well as the fraction of time spent as OB star + BH system compared to the total lifetime. We multiply the probability to observe a certain system resulting from the weighting in Section 3.3 with the respective computed time fraction. The top panel of Figures 10 to 13 each shows the distribution function taken the time spent as OB+BH system into account.

The time that a system spends as a binary composed of two main sequence stars increases with an increasing initial mass ratio. Therefore, secondary stars with a high mass become more unlikely to be observed in an OB star + BH system. This explains the strong decrease in Figure 10 for OB star masses exceeding $20\,M_\odot$ compared to Figure 4. As we have already stated, systems undergoing case A mass transfer originate mostly from grids with high initial primary masses. Models with a high initial mass ratio are more likely to undergo stable mass transfer when both stars are still on their main sequence while close systems with a low mass ratio mostly evolve into a common envelope system. Therefore, binaries with a lower orbital period and a higher radial velocity semi-amplitude of the OB star are less likely to be observed in an OB star + BH binary. The influence of the mass ratio on the time spent as MS + MS binary can be seen directly in Figure 13. The peak is clearly shifted towards lower final mass ratios compared to Figure 6.

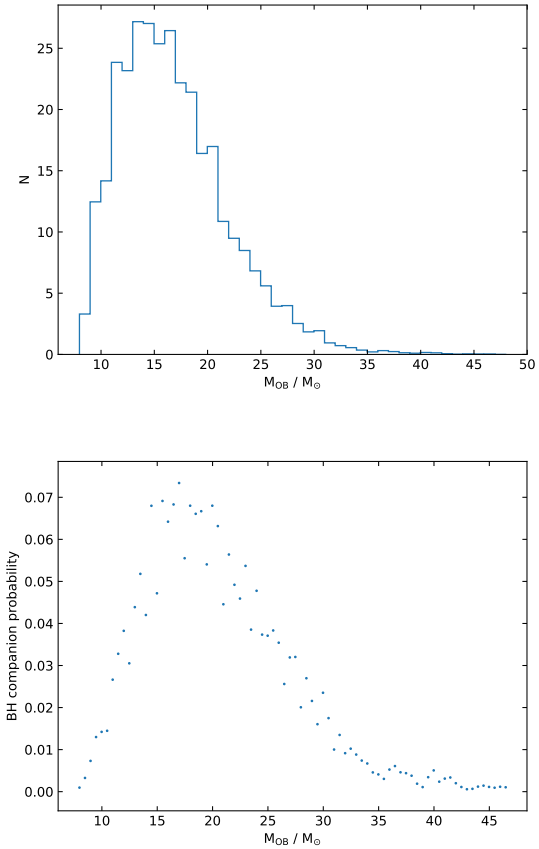

Figure 10: (top) Distribution of the OB star masses with the time spent as OB star + BH system taken into account. Initial distribution functions are taken into account according to Section 3.3.
(bottom) Each dot shows the number of OB star + BH systems containing an OB star of the stated mass as a fraction of the number of stars according to the initial distribution function considering the time spent as MS + MS system in the respective bin.

We compare the resulting distribution functions to the total distribution functions of OB stars for the mass and the radial velocity and to the total distribution functions of binaries for period and mass ratio. As a first approximation, we use the initial distribution functions as noted in Section 3.3 and stack the probability of systems in each bin of the distribution function for MS + MS systems to the respective bin of the initial distribution function. Therefore we take into account that a system which exists mostly as a MS + MS binary is unlikely to be observed as an OB star + BH binary even if it will evolve into such a system for a rather short period of time.
The bottom panels of Figures 10 to 13 show the number of systems in each bin of the respective top panel as a fraction of the number of systems in the bin of the total distribution function computed as described above.

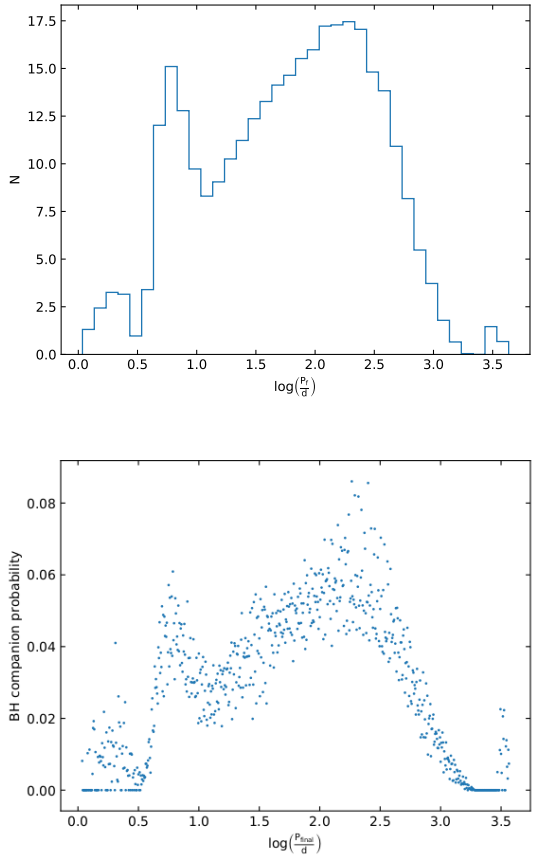

Figure 11: (top) Distribution of the orbital periods with the time spent as OB star + BH system taken into account. Initial distribution functions are taken into account according to Section 3.3.
(bottom) Each dot shows the number of OB star + BH systems of the stated orbital period as a fraction of the number of stars according to the initial distribution function considering the time spent as MS + MS system in the respective bin.

We can therefore read off the ordinate the probability for an OB star or a system with the observed value of the parameter on the abscissa to be in a binary with a BH.
The plots suggest that it is most likely for an OB star in a mass range of $15-20\,M_\odot$ and a radial velocity semi-amplitude of either $50\,\frac{km}{s}$ or $100\,\frac{km}{s}$ to have a BH as a companion. Furthermore, systems with an orbital period of either $\log(P/d) \approx 0.8$ ($P = 6.3\,d$) or $\log(P/d) \approx 1.5 - 2.5$ ($P = 32 - 316\,d$) and a mass ratio in the range of $q = 1.0$ and $q = 1.5$ have the highest probability to be an OB star + BH system.

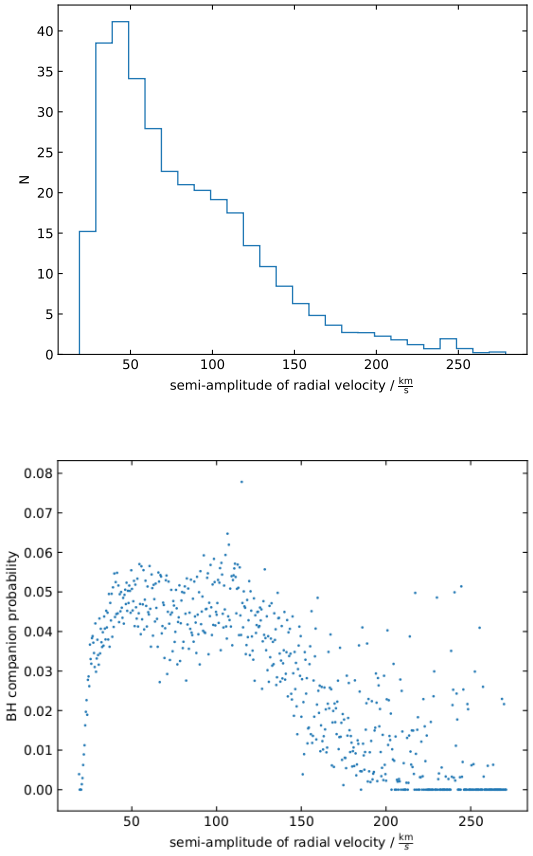

Figure 12: (top) Distribution of the radial velocity semi-amplitudes with the time spent as OB star + BH system taken into account. Initial distribution functions are taken into account according to Section 3.3. (bottom) Each dot shows the number of OB star + BH systems containing an OB star of the stated radial velocity semi-amplitude as a fraction of the number of stars according to the initial distribution function considering the time spent as MS + MS system in the respective bin.

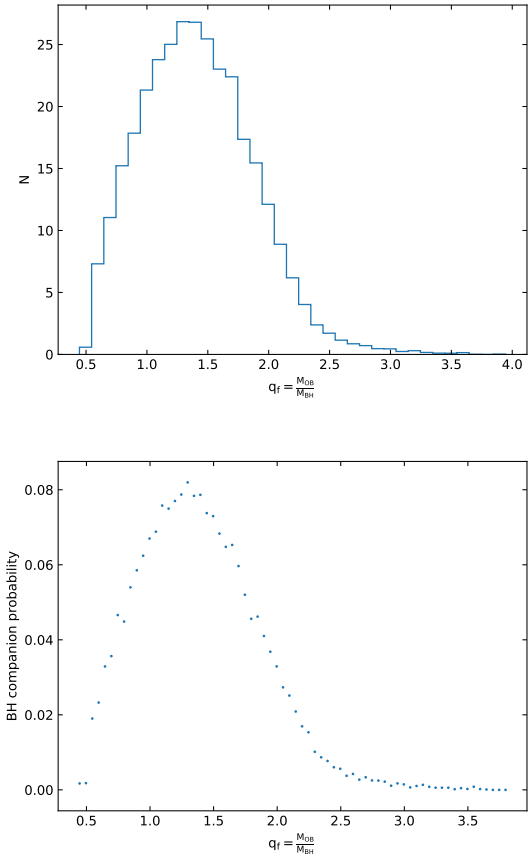

Figure 13: (top) Distribution of the mass ratios with the time spent as OB star + BH system taken into account. Initial distribution functions are taken into account according to Section 3.3.
(bottom) Each dot shows the number of OB star + BH systems of the stated mass ratio as a fraction of the number of stars according to the initial distribution function considering the time spent as MS + MS system in the respective bin.

4.4 Properties of the OB stars

Figure 14 shows the rotational velocity distribution of the OB stars and Figure 15 shows the distribution of the rotational velocity as a fraction of the critical rotational velocity. Non-interacting systems are not rotating as they did not speed up through mass transfer. The OB stars that underwent case A mass transfer and especially those in contact systems accreted mass but are slowed down due to tidal forces as they are very close binaries. Therefore these systems can accrete a high amount of mass without reaching their critical rotational velocity.
In case B systems, the OB stars accrete mass but the stars are not tidally locked and thus not slowed down. For most of these systems and three of our case B example systems, the OB stars rotate almost with their critical rotational velocity which prevents them from accreting further mass. The OB stars that rotate at less than 90 % of their

critical rotational velocity but also underwent case B mass transfer probably suffer from wind mass loss and are therefore slowed down. Most of the OB stars coming from case A system rotate with a rather small fraction of their critical rotational velocity, especially the one in system 5 (blue square) which is a contact system.
The described effects are also visible in Figure 16 which shows the rotational velocities of the OB stars separated by their different masses. OB stars with a higher mass tend to have a lower rotational velocity whereas the stars with the lowest mass almost all rotate very fast. As the number of systems undergoing case A mass transfer increases for an increasing initial mass of the primary which also means a higher initial mass possible for the secondary. This matches our previously discussed results.

Figures 17 and 18 show the helium and nitrogen surface abundances of the OB stars as a fraction of their initial helium or nitrogen abundance. For most of the OB stars, the surface abundances did not change much, in particular for those coming from case B systems. OB stars that accreted a high amount of mass from the primary star however have a surface that is enriched in helium and especially in nitrogen. The OB star originating from the contact system (blue square) shows a nitrogen abundance that is approximately ten times higher than its initial abundance.
Therefore, an observed OB star that is nitrogen or helium enriched could be an indication for a black hole being the second component of the binary.

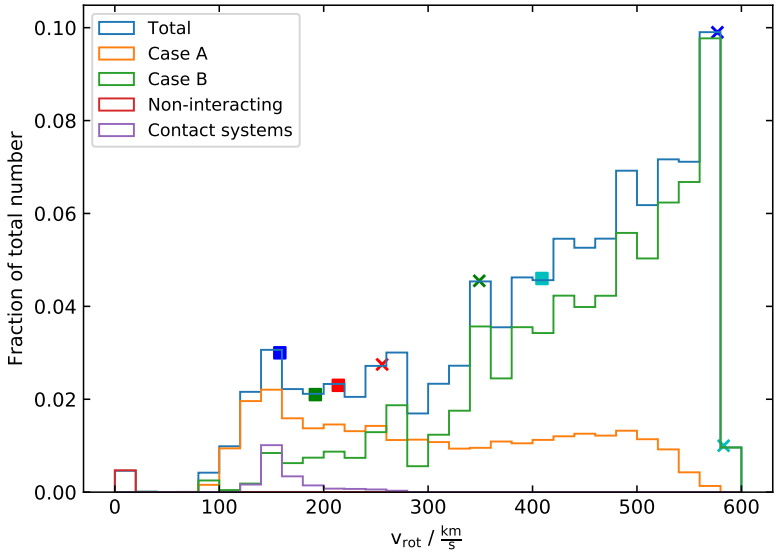

Figure 14: Distribution of the resulting rotational velocities of the OB stars. Initial distribution functions are taken into account according to Section 3.3. For parameters of the example systems see Table 1.

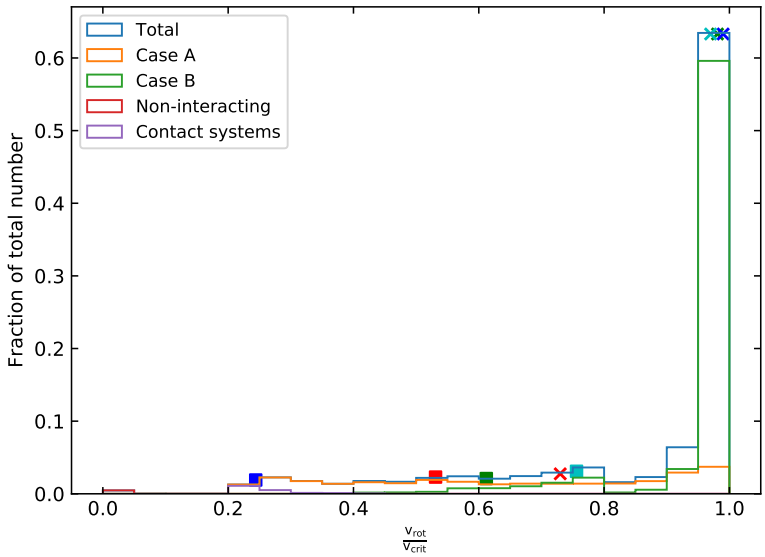

Figure 15: Distribution of the resulting rotational velocities of the OB stars as a fraction of their critical rotational velocities. Initial distribution functions are taken into account according to Section 3.3. For parameters of the example systems see Table 1.

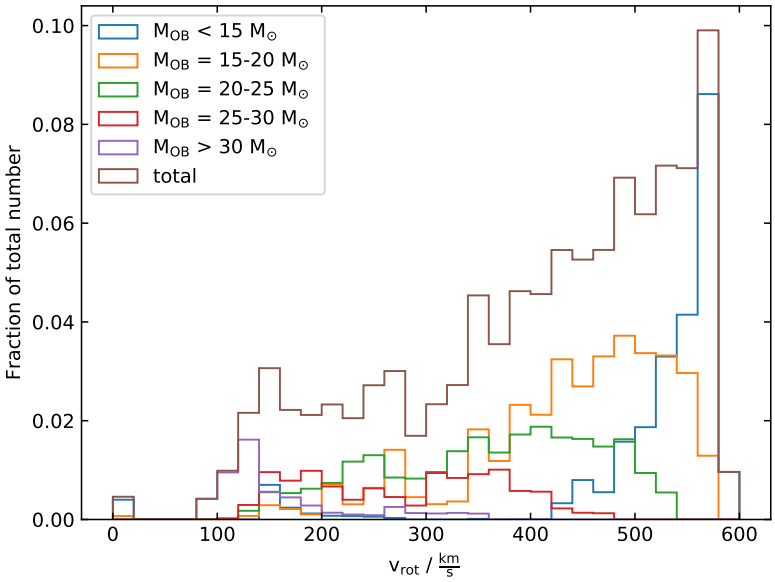

Figure 16: Distribution of the resulting rotational velocity dependent on the mass of the OB star. Initial distribution functions are taken into account according to Section 3.3.

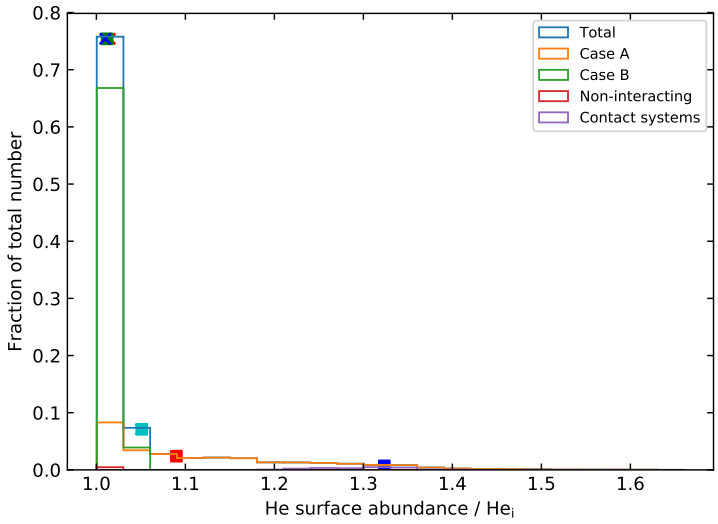

Figure 17: Distribution of the resulting helium surface abundance of the OB stars as a fraction of their inital helium abundance. Initial distribution functions are taken into account according to Section 3.3. For parameters of the example systems see Table 1.

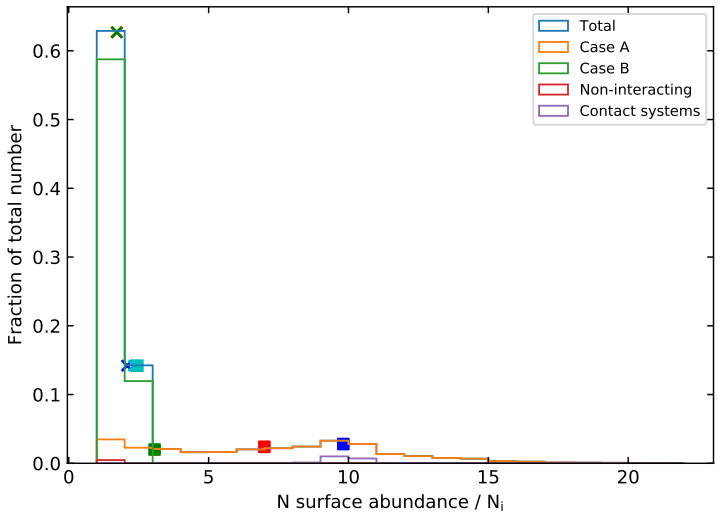

Figure 18: Distribution of the resulting nitrogen surface abundance of the OB stars as a fraction of their inital nitrogen abundance. Initial distribution functions are taken into account according to Section 3.3. For parameters of the example systems see Table 1.

4.5 Comparison to observed data

We compare the probability distributions for OB star + BH systems we derived in Section 4.3 to the observations that have been made so far.
Postnov and Yungelson (2014) list four binaries that consist of an O- or B-type star and a BH: Cygnus X-1, MWC 656, M33 X-7 and LMC X-1. Furthermore, Almeida et al. (2017) analysed observations of 51 single-lined O- or B-type binaries. Riedel (2018) identified four of these as possible OB star + BH binaries. The parameters of the eight systems are listed in Table 2. For MWC 656 we take the mean value of the respective denoted parameter range.

There are more observations of binaries consisting of a Wolf-Rayet and an OB star than of OB star + BH systems, see for example Foellmi et al. (2003). Hence we examine the properties of the systems that evolve into an OB star + BH binary at the point in time when the mass transfer stops, i. e. when they are still WR + OB binaries. We still take the time spent as OB star + BH system respectively MS + MS system into account, therefore the ordinates for the OB star + WR star systems in the Figures 19 and 22 give the probability to observe a detected WR + OB system with a certain mass ratio respectively OB star mass as an OB star + BH system later.

The mass of the O-type star in Cyg X-1 is very close to the predicted mass for which an OB-type star would have the highest probability to be in a binary with a BH (see Figure 19). The masses of the possible candidates from the VFTS survey are slightly higher than the predicted interval of $15 - 20\,\mathrm{M}_\odot$. However the mass of those stars is not very well constrained and might therefore differ from the calculations by Riedel (2018). The O-type star in M33 X-7 has a much higher mass than the range that our models cover and can thus not be explained by our predictions.

Figure 20 shows the probability distribution for the orbital periods. Most of the systems match our predictions fairly well. According to our calculations, VFTS 064 and VFTS 332 would have a rather small probability to be OB star + BH systems since they have high orbital periods. For systems with a high initial orbital period that could evolve into systems with such high periods, there occured a convergence error for almost all those models from the grid. We would have to find a criterion to model the unstable mass transfer in these systems in order to get an estimate of their final parameters and therefore for the probability of the concerned parameter range. Furthermore, the initial orbital period reaches only up to $\log(\mathrm{P/d}) = 3.5$, so the systems might be explained by taking higher initial orbital periods into account.
M33 X-7 and LMC X-1 would also have a rather small detection probability as they are quite close systems but not close enough to be identified as contact systems.

The radial velocity semi-amplitude (see Figure 21) of all the observed OB stars lie in the parameter range for which we predict the highest probability for them to have a BH companion.

The mass ratios (see Figure 22) of Cygnus X-1 as well as those of the systems analysed by the VFTS match our predictions pretty well. MWC 656, M33 X-7 and LMC X-1 however have very high OB star masses compared to the mass of the respective BH. Here we might take into account that we assumed the BH masses to be the mass of the former helium star which might result in lower mass ratios than the actual OB star to BH mass.
Furthermore, it should be considered that the observed systems might have a different metallicity than the assumed LMC metallicity which can lead to further deviations.

At an earlier point in time, when the primary still exists as a WR star, the masses of the OB stars as well as the mass ratios for whose the system is most likely to be observed as OB star + BH system do not differ significantly from those derived directly for the OB star + BH systems. The curve of the mass ratios is slightly shifted towards lower values, which would mean a higher mass of the companion if the OB star mass remains constant as suggested by Figure 19. Therefore the WR star would still lose a small fraction of its mass during the evolution into a BH.

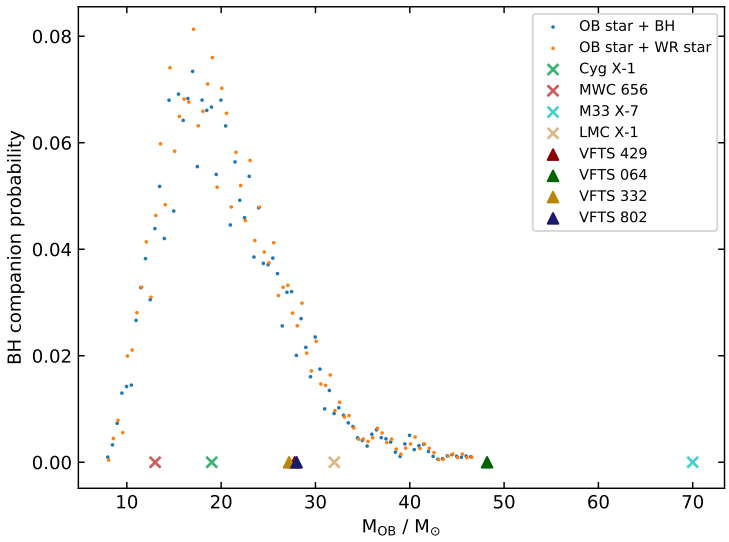

Figure 19: Each dot shows the number of OB star + BH systems and WR star + OB star systems containing an OB star of the stated mass as a fraction of the number of stars according to the initial distribution function considering the time spent as MS + MS system in the respective bin (see Section 4.3). The approximate masses of the OB stars in the observed systems and possible candidates from the VFTS are marked.

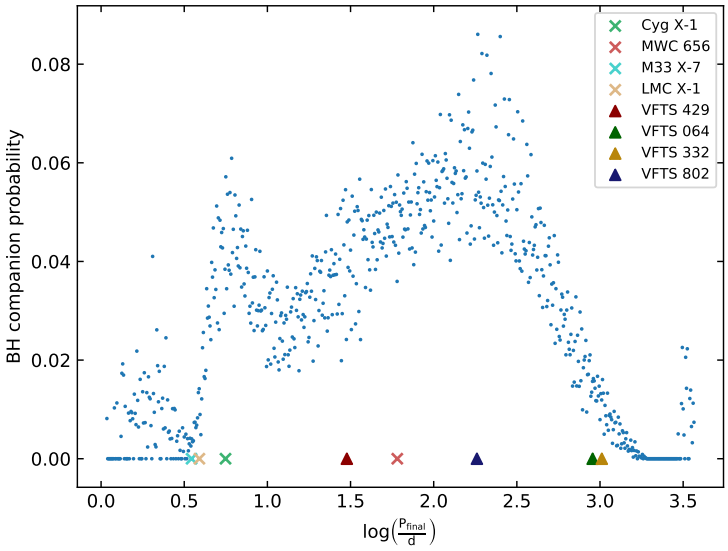

Figure 20: OB star + BH systems having the stated orbital period as a fraction of the initial distribution function considering the time spent as MS + MS system (see Section 4.3). The approximate orbital periods of the observed systems and possible candidates from the VFTS are marked.

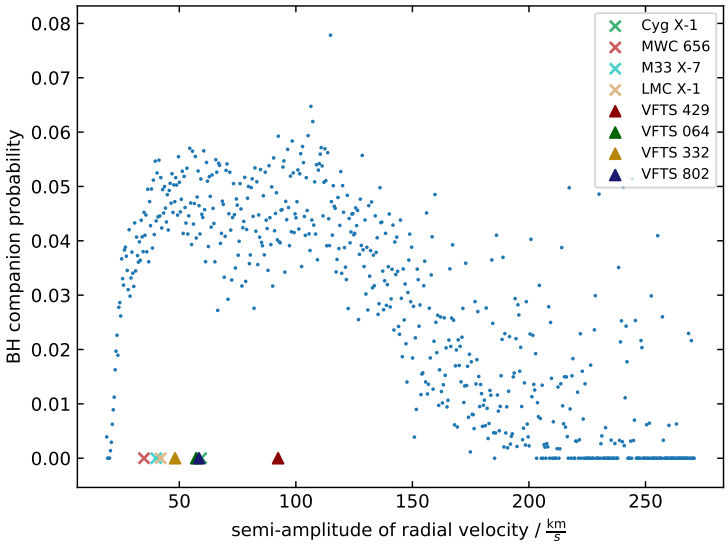

Figure 21: Each dot shows the number of OB star + BH systems containing an OB star of the stated radial velocity semi-amplitude as a fraction of the number of stars according to the initial distribution function considering the time spent as MS + MS system in the respective bin (see Section 4.3). The radial velocities of the OB stars in the observed systems and possible candidates from the VFTS are marked.

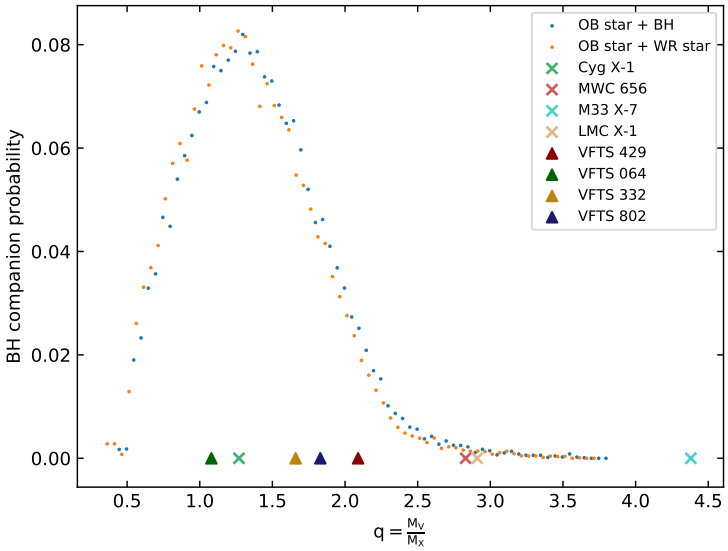

Figure 22: Each dot shows the number of OB star + BH systems and WR star + OB star systems of the stated mass ratio as a fraction of the number of stars according to the initial distribution function considering the time spent as MS + MS system in the respective bin (see Section 4.3). The approximate mass ratios of the observed systems and possible candidates from the VFTS are marked.

5 Conclusion

In this work, we analysed the properties of OB star + BH systems based on the binary star data grid by Marchant (2016).
We found that an OB star has the highest probability to have a BH companion if it has a mass in the range of $15-20\,M_{\odot}$. With the exception of M33 X-7, the present observations match this predicted mass range quite well. Especially VFTS 429, VFTS 332 and VFTS 802 seem to be good candidates for OB star + BH systems according to their OB star mass. Furthermore, systems with an orbital period of either $\log(P/d) \approx 0.8$ ($P = 6.3\,d$) or $\log(P/d) \approx 1.5 - 2.5$ ($P = 32 - 316\,d$) have the highest probability to be OB star + BH systems. This is supported by the observations of Cyg X-1 and MWC 656 and would mean a high chance for VFTS 429 and VFTS 802 to be such systems. From the masses of the two components and the orbital period we computed the semi-amplitude of the radial velocity of the OB star and found that OB stars with a radial velocity semi-amplitude of either $50\,\frac{km}{s}$ or $100\,\frac{km}{s}$ are most likely to have a BH companion. These values are close to the values of the observed OB stars that have BH companions and suggest for all of the VFTS candidates to be OB star + BH systems. Considering the mass ratio, systems with an OB star to BH mass ratio in the range of $q = 1.0$ and $q = 1.5$ have the highest probability to be OB star + BH systems. This can only be confirmed by the observed mass ratio of Cyg X-1. The other observed OB star + BH systems either have a too small BH mass or a too massive OB star to match our predictions. VFTS 064, VFTS 332 and VFTS 802, especially, are good OB star + BH candidates according to their mass ratios.
Furthermore, we worked out that a large fraction of OB stars with a BH companion rotate with almost their critical rotational velocity. A rather small fraction of these stars show enriched helium or nitrogen surface abundances. Therefore, a high rotational velocity or a strong helium or nitrogen surface abundance of an observed OB star could be an indicator for it to have undergone binary interaction and to have a BH companion.

References

Abbott, B. P. et al. (2016). "Observation of Gravitational Waves from a Binary Black Hole Merger". In: *Phys. Rev. Lett.* 116, p. 061102.

Almeida, A. L., H. Sana, W. Taylor, R. Barbá, A. Z. Bonanos, P. Crowther, A. Damineli, A. de Koter, S. E. de Mink, C.J. Evans, M. Gieles, N. J. Grin, V. Hénault-Brunet, N. Langer, D. Lennon, S. Lockwood, J. Maíz Apellániz, A. F. J. Moffat, C. Neijssel, C. Norman, O. H. Ramírez-Agudelo, N. D. Richardson, A. Schootemeijer, T. Shenar, I. Soszynski, F. Tramper, and J. S. Vink (2017). "The Tarantula Massive Binary Monitoring: I. Observational campaign and OB-type spectroscopic binaries". In: *Astronomy & Astrophysics* 598.

Ertl, T., H.-Th. Janka, S.E. Woosley, T. Sukhbold, and M. Ugliano (2016). "A two-parameter criterion for classifying the explodability of massive stars by the neutrino-driven mechanism". In: *The Astrophysical Journal* 818, 23pp.

Foellmi, C., A. F. J. Moffat, and M. A. Guerrero (2003). "Wolf-Rayet binaries in the Magellanic Clouds and implications for massive-star evolution - II. Large Magellanic Cloud". In: *Monthly Notice of the Royal Astronomical Society* 338, pp. 1025–1056.

Marchant, P. (2016). "The impact of tides and mass transfer on the evolution of metal-poor massive binary stars". Dissertation. Rheinische Friedrich-Wilhelms-Universität Bonn. URL: `https://astro.uni-bonn.de/~nlanger/thesis/pablo.pdf`.

Müller, B., A. Heger, D. Liptai, and J. B. Cameron (2016). "A simple approach to the supernova progenitor-explosion connection". In: *Monthly Notices of the Royal Astronomical Society* 460, pp. 742–764.

Paxton, B., L. Bildsten, A. Dotter, F. Herwig, P. Lesaffre, and F. Timmes (2011). "Modules for Experiments in Stellar Astrophysics (MESA)". In: *The Astrophysical Journal Supplement* 192, 35pp.

Pols, O. R. (2009). *Stellar Structure and Evolution.*

Postnov, K. A. and L. R. Yungelson (2014). "The Evolution of Compact Binary Star Systems". In: *Living Rev. Relativity* 17.

Riedel, W. (2018). "On the Invisible Component of Massive Single Line Spectroscopic Binaries". Bachelor Thesis. Rheinische Friedrich-Wilhelms-Universität Bonn. URL: `https://astro.uni-bonn.de/~nlanger/thesis/RiedelBachelor.pdf`.

Salpeter, E. E. (1955). "The luminosity function and stellar evolution". In: *The Astrophysical Journal* 121, p. 161.

Sana, H., S. E. de Mink, A. de Koter, N. Langer, C. J. Evans, M. Gieles, E. Gosset, R. G. Izzard, J.-B. Le Bouquin, and F. R. N. Schneider (2012). "Binary interaction dominates the evolution of massive stars". In: *Science* 337.

Sukhbold, T., W. E. Woosley, and A. Heger (2018). "A High-resolution Study of Presupernova Core Structure". In: *The Astrophysical Journal* 860, 22pp.

List of Figures

List of Tables

6 Appendix

Table 1: Sample systems

system	1	2	3	4	5	6	7	8
$M_{1,i}/M_\odot$	19.95	19.95	25.12	25.12	31.62	35.48	39.81	39.81
q_i	0.900	0.925	0.875	0.925	0.300	0.400	0.275	0.300
$\log(P_i/d)$	0.525	0.900	2.675	0.950	0.175	1.350	1.375	3.075
mass transfer	case A	case B	case B	case A	case A	case B	case A	case B
$M_{BH}/M_\odot$	7.273	8.406	11.72	11.087	10.008	16.417	17.616	20.371
$M_{OB}/M_\odot$	23.032	18.718	21.915	23.644	11.041	8.231	11.530	12.478
q_f	3.167	2.227	1.871	2.133	1.086	0.869	0.655	0.613
$\log(P_f/d)$	0.940	1.153	3.081	1.205	0.181	0.976	0.547	2.500
$K_{2,f}$ / $\frac{km}{s}$	77	82	22	88	246	171	260	62
age / Myr	10.55	10.16	7.96	7.98	7.16	5.91	5.46	5.43
$v_{rot,2,f}/\frac{km}{s}$	214	256	349	192	158	577	469	583
$\frac{v_{rot,2,f}}{v_{crit,2,f}}$	0.531	0.73	0.981	0.612	0.244	0.99	0.756	0.97
surface ^{14}N / $^{14}N_i$	6.99	1.72	1.72	3.07	9.82	2.09	2.45	2.33
surface ^4He / ^4He_i	1.10	1.01	1.01	1.01	1.32	1.01	1.05	1.05
$H_{center,2}$	0.011	0.078	0.133	0.053	0.633	0.567	0.642	0.626

Table 2: Parameters of the observed OB star + BH binaries from Table 4 of Postnov and Yungelson (2014). The last four systems were analysed as part of the VFTS survey (Almeida et al. (2017)) and identified as possible binaries containing a BH by Riedel (2018) (orbital periods and radial velocities according to Almeida et al. (2017), masses and mass ratio according to Riedel (2018)).

system	Cyg X-1	MWC 656	M33 X-7	LMC X-1	429	064	332	802
P / d	5.6	60.4	3.5	3.9	30.0439	902.9	1025.3	181.883
$M_x/M_\odot$	15	3.8 - 6.9	16	11	13.3	44.7	16.4	15.2
$M_v/M_\odot$	19	10 - 16	70	32	27.8	48.2	27.2	27.8
q	1.27	1.45 - 4.21	4.38	2.91	2.09	1.08	1.66	1.83
$K_2/\frac{km}{s}$	59.4	28.6 - 41.1	40.1	42.0	92.37	57.22	48.17	58.46

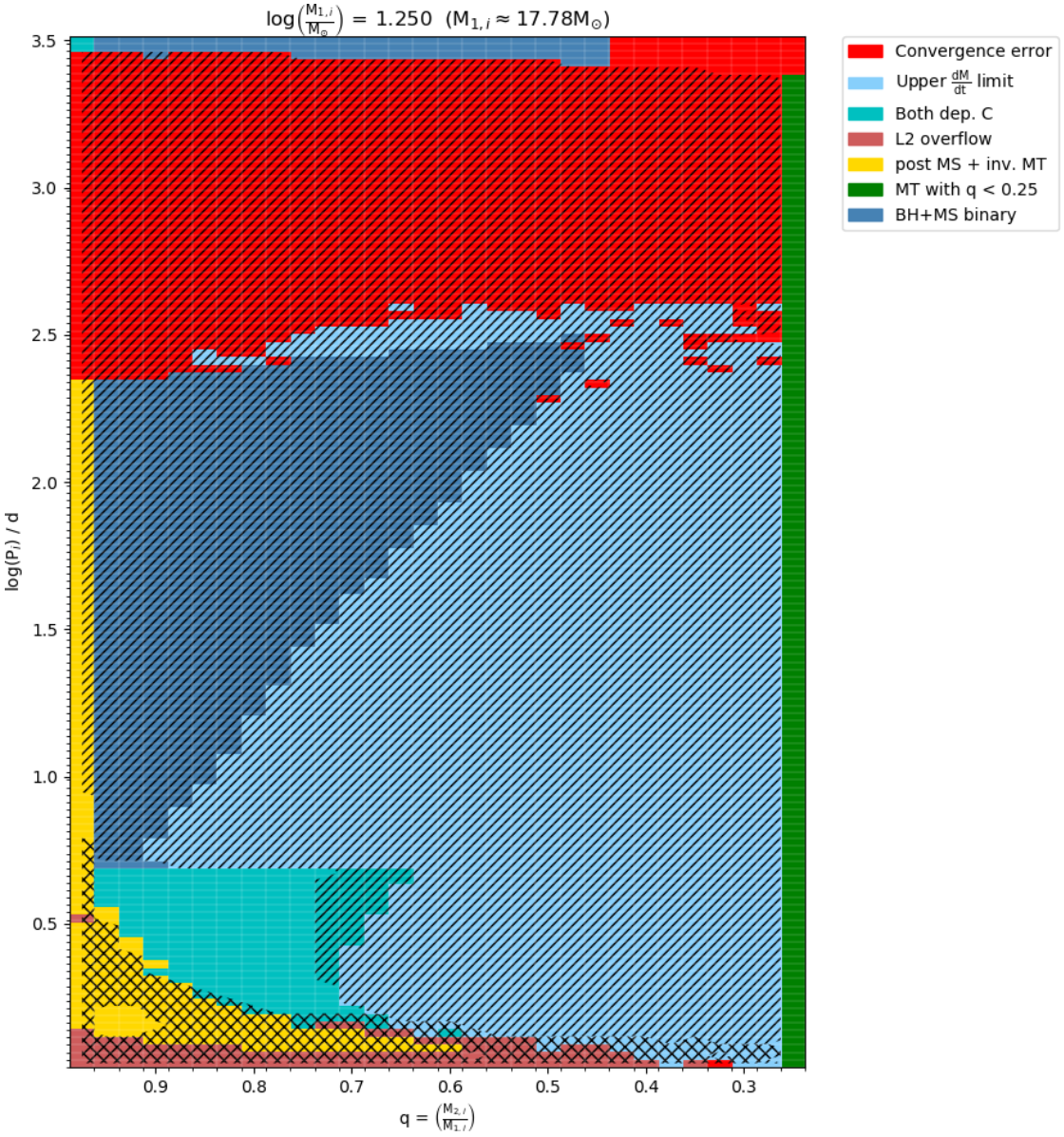

Figure 23: Grid of binary models for $\log\left(M_{1,i}/M_{\odot}\right) = 1.250$. See Section 4.1 for detailed explanation.

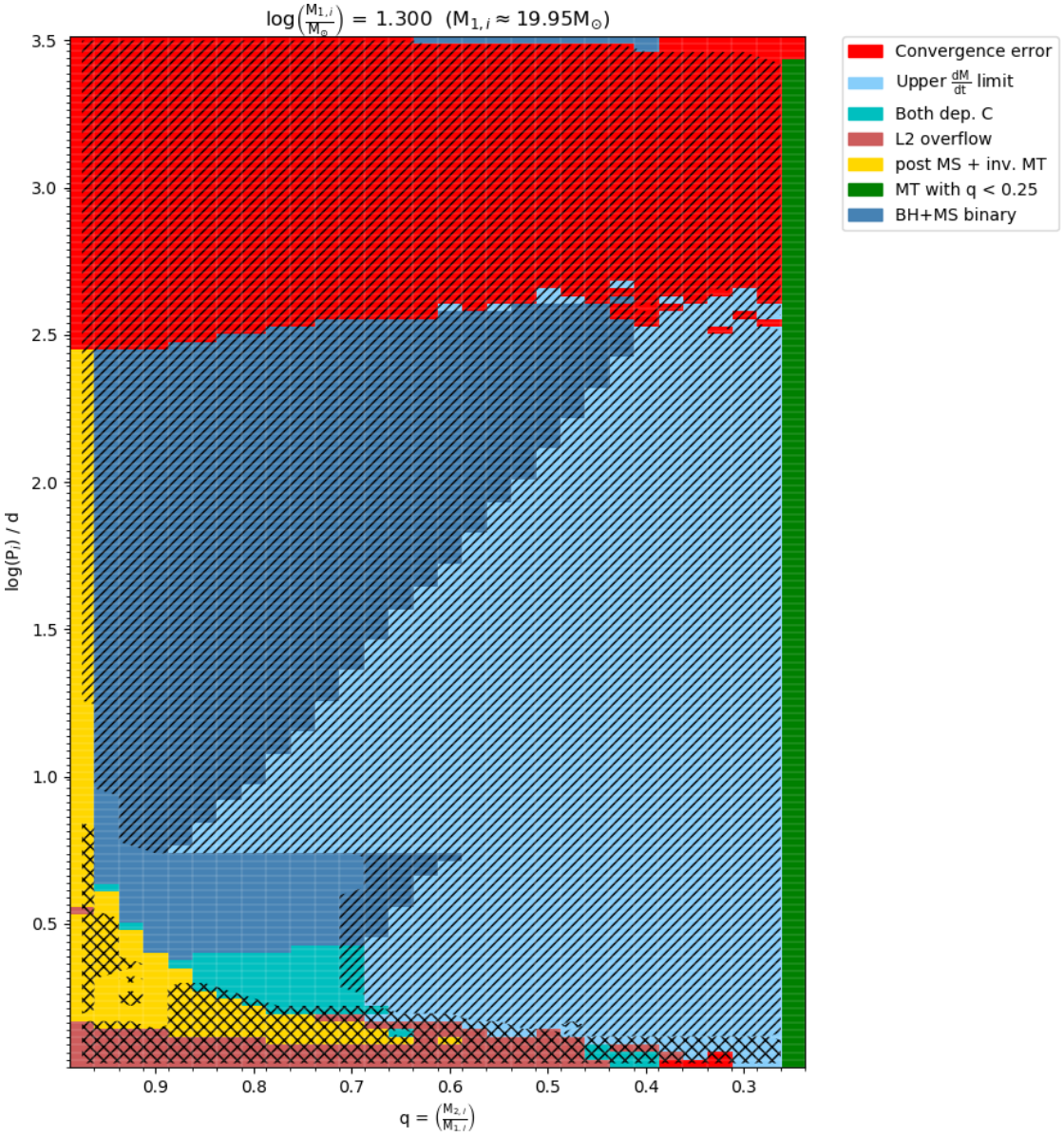

Figure 24: Grid of binary models for $\log\left(M_{1,i}/M_{\odot}\right) = 1.300$. See Section 4.1 for detailed explanation.

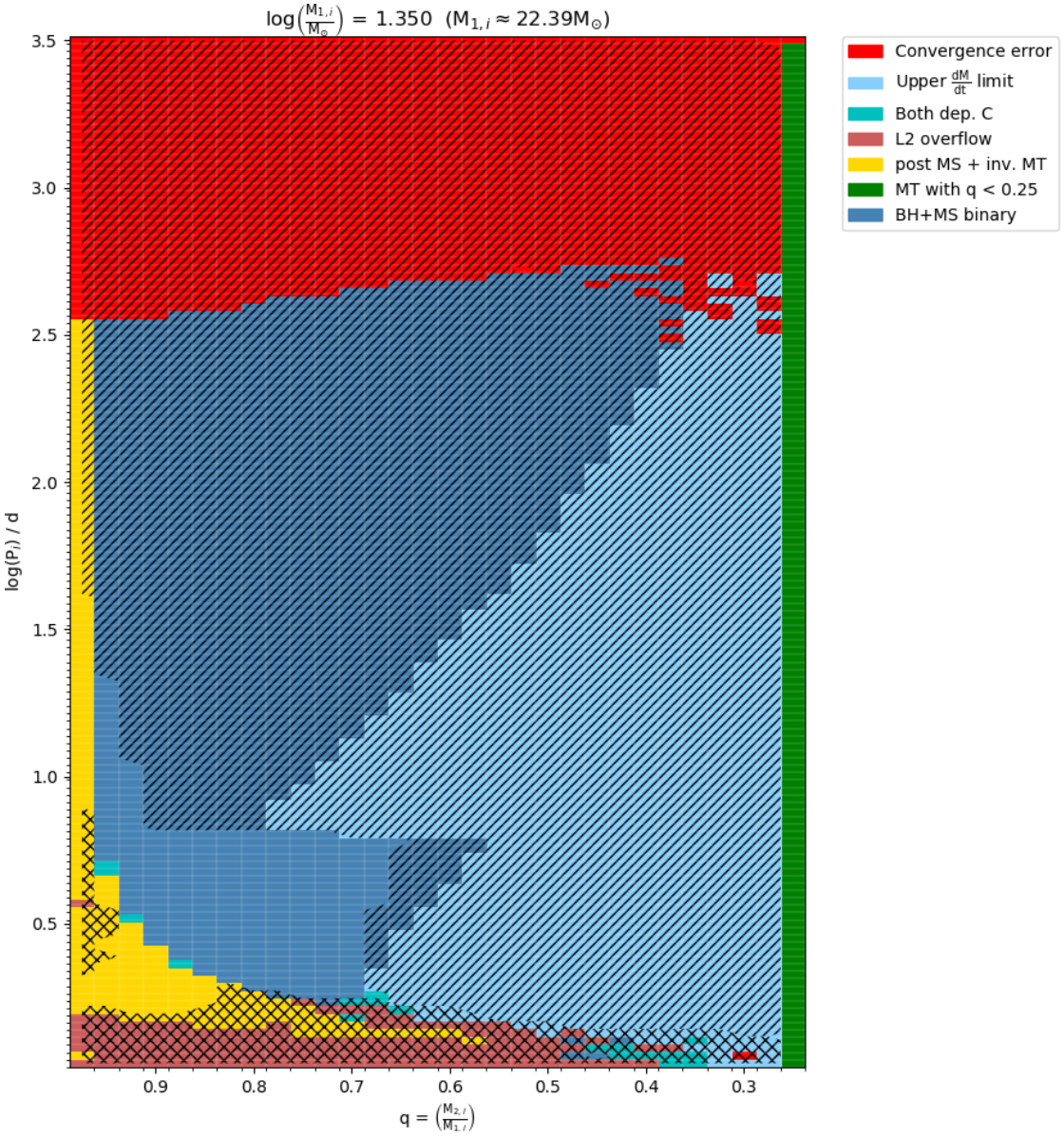

Figure 25: Grid of binary models for $\log\left(M_{1,i}/M_{\odot}\right) = 1.350$. See Section 4.1 for detailed explanation.

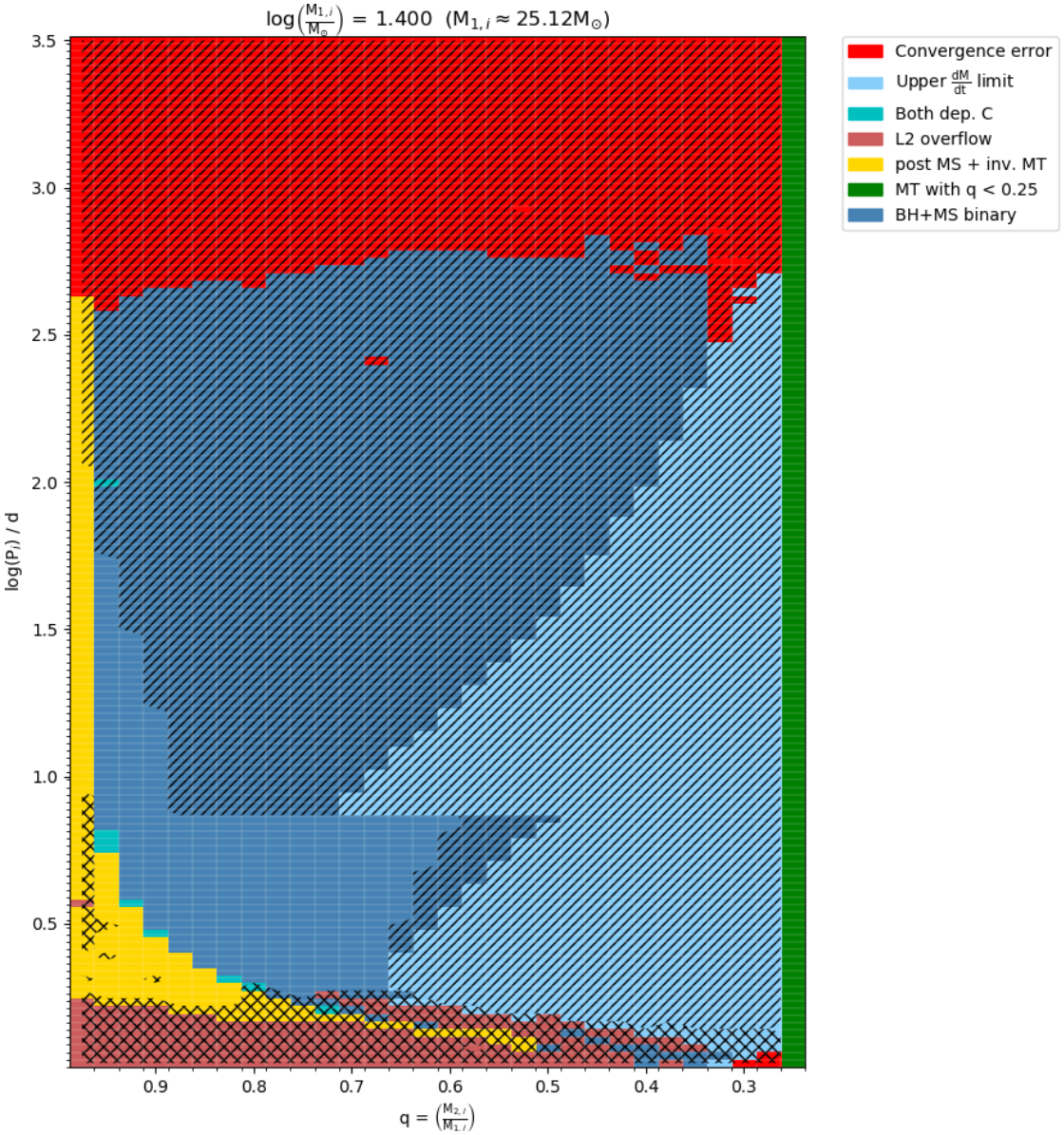

Figure 26: Grid of binary models for $\log\left(M_{1,i}/M_{\odot}\right) = 1.400$. See Section 4.1 for detailed explanation.

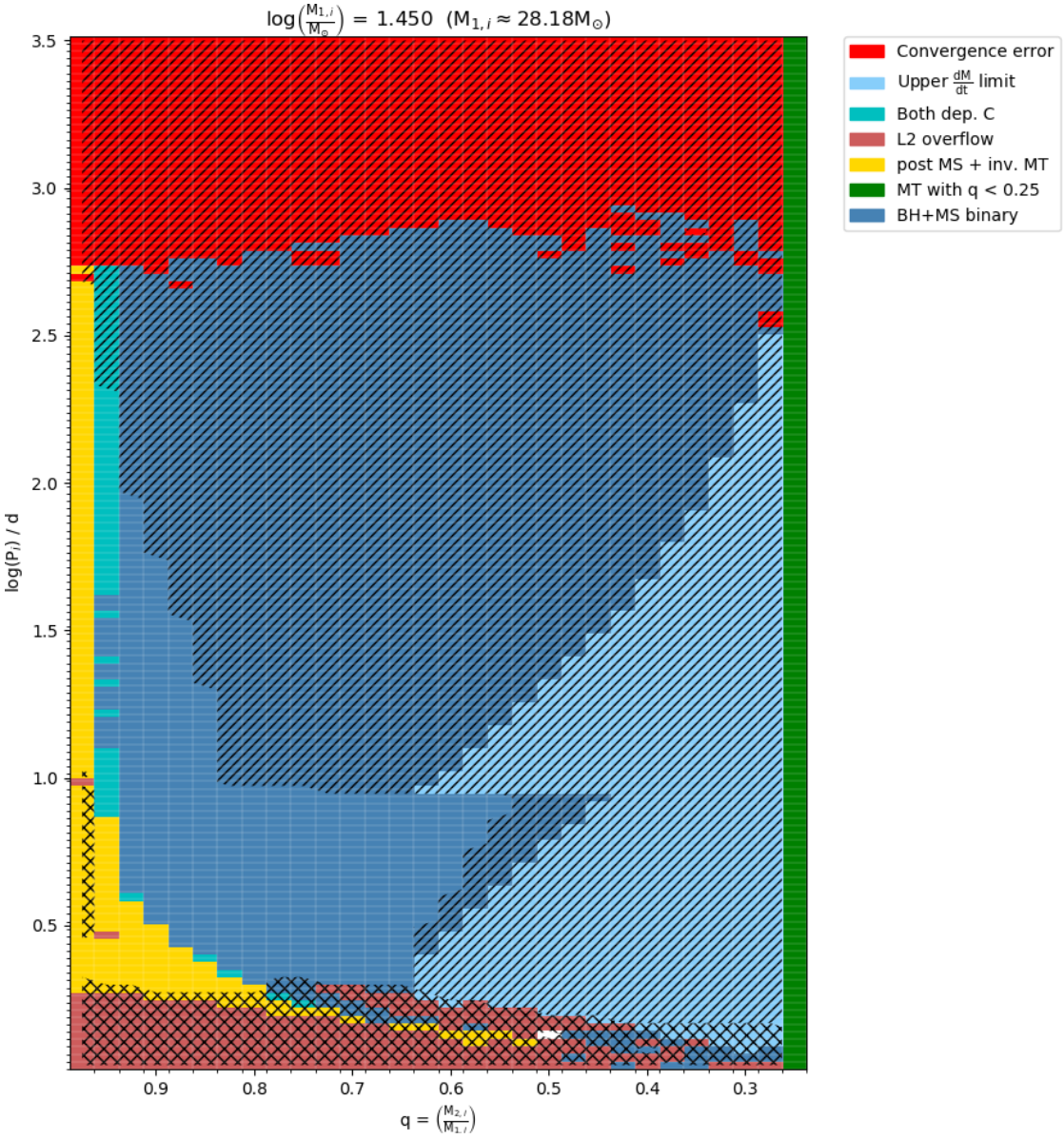

Figure 27: Grid of binary models for $\log\left(M_{1,i}/M_{\odot}\right) = 1.450$. See Section 4.1 for detailed explanation.

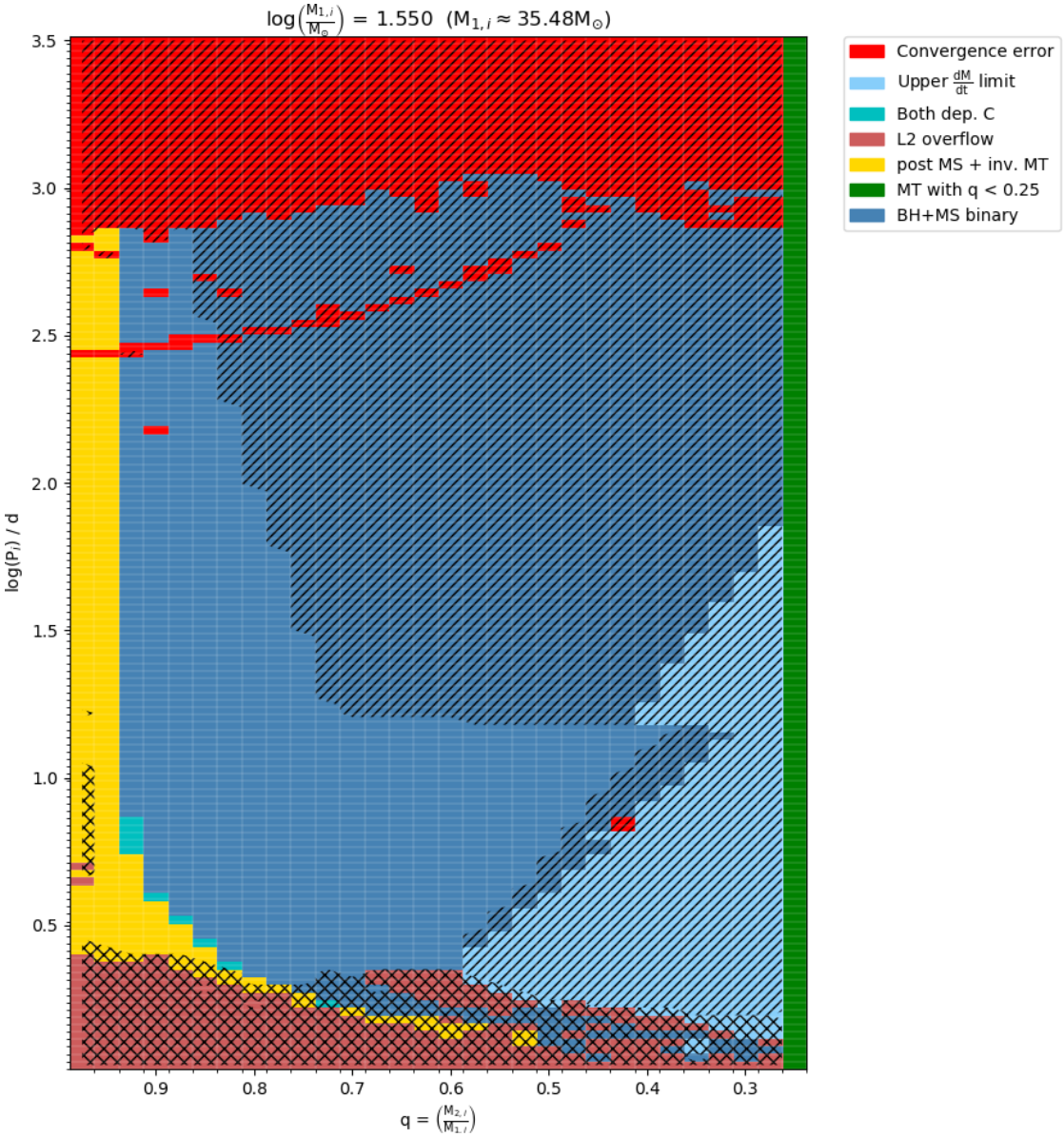

Figure 28: Grid of binary models for $\log\left(M_{1,i}/M_{\odot}\right) = 1.550$. See Section 4.1 for detailed explanation.

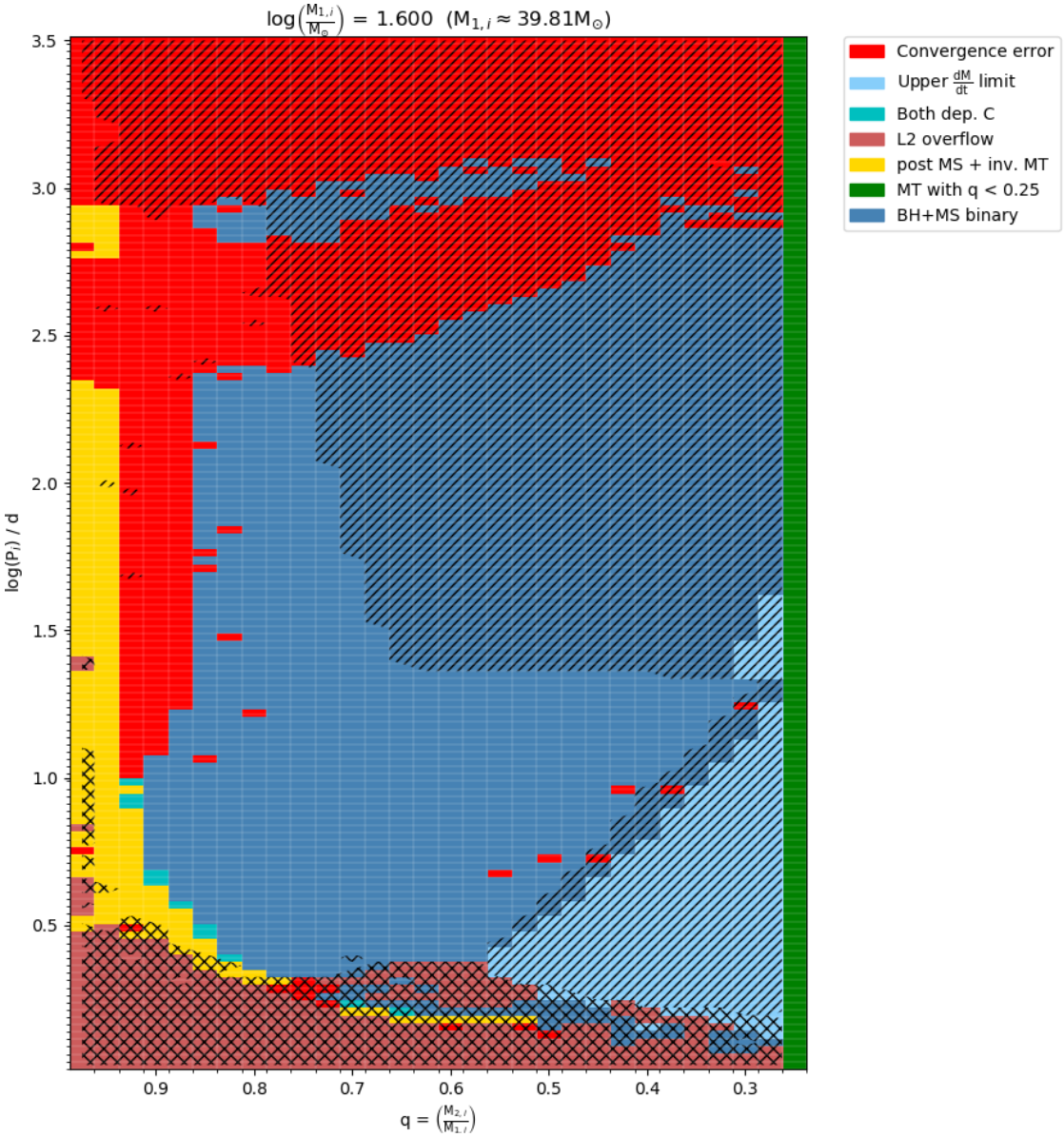

Figure 29: Grid of binary models for $\log\left(M_{1,i}/M_{\odot}\right) = 1.600$. See Section 4.1 for detailed explanation.